Research Square

Preprints are preliminary reports that have not undergone peer review.
They should not be considered conclusive, used to inform clinical practice,
or referenced by the media as validated information.

Task-Evoked Metabolic Balance and Intrinsic Network Organization Relate to Processing Speed

Antonia Kaiser

antonia.kaiser@epfl.ch

1) CIBM Center for Biomedical Imaging, Lausanne, Switzerland 2) Metabolic Magnetic Resonance Spectroscopy (MetMRS) Group, Ecole Polytechnique Fédérale de Lausanne (EPFL), Lausanne, Swi
https://orcid.org/0000-0001-7805-6766

Ying Xiao

École Polytechnique Fédérale de Lausanne

Ines Khadimallah

Center for Psychiatric Neuroscience, Department of Psychiatry, Lausanne University Hospital (CHUV), Lausanne, Switzerland https://orcid.org/0000-0001-7040-4455

Mark Widmaier

1) CIBM Center for Biomedical Imaging, Lausanne, Switzerland 2) Metabolic Magnetic Resonance Spectroscopy (MetMRS) Group, Ecole Polytechnique Fédérale de Lausanne (EPFL), 6) Department

Yan Lin

Radiology Department, Second Affiliated Hospital, Shantou University Medical College, China
https://orcid.org/0000-0002-8284-9029

Daniel Wenz

Animal Imaging and Technology, École polytechnique fédérale de Lausanne

Dimitrios Karampinos

1) CIBM Center for Biomedical Imaging, Lausanne, Switzerland 2) Metabolic Magnetic Resonance Spectroscopy (MetMRS) Group, Ecole Polytechnique Fédérale de Lausanne (EPFL), Lausanne, Swi

Kim Do

Center for Psychiatric Neuroscience https://orcid.org/0000-0003-1968-1646

Lijing Xin

EPFL https://orcid.org/0000-0002-5450-6109

Article

Keywords:

Posted Date: November 4th, 2026

DOI: https://doi.org/10.21203/rs.3.rs-11597882/v1

License: This work is licensed under a Creative Commons Attribution 4.0 International License.
Read Full License

Additional Declarations: There is **NO** Competing Interest.

Abstract

Processing speed is a core component of cognition that declines with aging and is impaired across neurological and psychiatric disorders. We combined functional proton magnetic resonance spectroscopy at 7 T with resting-state functional MRI to examine neurochemical and functional correlates of processing speed in 26 young and eight older adults. During a symbol–digit matching task, lactate showed a significant age-by-condition interaction, with a larger stimulation-related increase in older adults. Glutamate showed no significant group-level modulation, although its time course suggested a delayed response in older adults. The glutamate-to-lactate ratio decreased during stimulation in older adults, with an apparent rise during subsequent control periods, suggesting a possible temporal offset between the metabolite responses. Across participants, larger task-evoked lactate changes were associated with slower processing, whereas glutamate responses were heterogeneous and nonsignificant at the group level. Older adults also showed lower intrinsic functional coherence in the dorsal medial anterior cingulate cortex and executive and attention networks. Exploratory analyses linked greater coherence to better processing speed and smaller lactate responses. Together, these findings link individual differences in processing speed to both task-evoked neuroenergetic responses and intrinsic functional organization. The greater lactate recruitment observed with aging and poorer cognitive performance may reflect increased reliance on non-oxidative metabolism or compensatory metabolic engagement to meet cognitive demands. These results highlight fMRS as a complementary approach for characterizing the metabolic mechanisms underlying individual differences in cognition and cognitive aging.

Introduction

Cognitive functioning encompasses mental abilities including perception, attention, memory, and reasoning. Processing speed, the rate at which information is perceived, integrated, and acted upon[1,2], is a fundamental component of overall cognitive capacity[3,4] that supports higher-order functions such as executive control, working memory, and decision-making [5].

Impairments in processing speed are among the most consistent and functionally relevant deficits observed across both clinical and aging populations [6]. Marked slowing is evident in disorders such as schizophrenia, depression, and early psychosis [7–13]. Similarly, age-related declines in processing speed contribute substantially to impairments in attention, memory, and executive function [14]. Processing speed may therefore provide a sensitive behavioral index of cognitive and neural efficiency [15,16]. Despite its central importance, however, the neurobiological mechanisms underlying individual differences in processing speed remain incompletely understood.

Efficient cognitive processing depends on close coupling between neurotransmission and energy metabolism. Excitatory signaling, predominantly mediated by glutamate, imposes substantial energetic demands. These demands are met through rapid metabolic adaptations, including increased glycolysis

and the production of lactate, which may support neuronal and synaptic function [17–20]. Glutamate and lactate therefore provide complementary indicators of changes via oxidative and glycolytic pathways during cognitive demand [21–23]. Together, they provide a window into the neuroenergetic processes supporting rapid information processing [5,24].

However, direct in vivo evidence linking these neurochemical dynamics to cognitive function in humans remains scarce [25,26]. Most neuroimaging approaches, including functional MRI and PET, capture indirect or temporally limited proxies of neural activity, leaving the biochemical processes underlying cognition unclear [27].

Functional Magnetic Resonance Spectroscopy (fMRS) addresses this gap by enabling the in vivo measurement of activity-dependent changes in metabolites involved in neural function, including e.g. glutamate, lactate, γ-aminobutyric acid, and glutathione [28,29]. At 7 T, increased signal-to-noise ratio and spectral dispersion improve the separation of overlapping metabolite resonances and facilitate the detection of small task-related changes. Task-related changes in glutamate and lactate have been observed during sensory and cognitive stimulation, demonstrating sensitivity to excitatory engagement and metabolic demand [30–32]. These findings suggest that fMRS is sensitive to activity-dependent changes in both excitatory neurotransmission and metabolic demand [31,33–35]. Nevertheless, the relationship between these neurochemical responses and individual cognitive capacity remains largely unexplored.

Cognitive functions such as processing speed arise from the coordinated activity of distributed brain networks [1,2]. The dorsal medial anterior cingulate cortex (dmACC) contributes to cognitive control and effort allocation under demand [36]. Resting-state functional MRI (rs-fMRI) complements fMRS by capturing large-scale network organization and intrinsic functional connectivity, offering a systems-level perspective on cognitive capacity [37]. Combining fMRS and resting-state functional MRI therefore enables local neurochemical engagement in the dmACC to be examined alongside the broader functional architecture supporting processing speed.

Here, we combined ultra-high-field (7T) fMRS with resting-state fMRI to investigate the neurochemical and functional correlates of processing speed. Participants performed a symbol–digit matching task while glutamate and lactate concentrations were measured continuously in the dmACC[36–39].

Our primary aim was to determine whether cognitive engagement elicits reproducible changes in glutamate and lactate and whether these responses vary with behavioral indicators of processing speed. The control condition required participants to read digits aloud at a matched presentation rate, contrast, and luminance, providing a stringent control for speech production, low-level visual stimulation, and nonspecific arousal. We additionally examined the glutamate-to-lactate ratio as an exploratory index of the balance between oxidative and glycolytic metabolism. To relate these local metabolic dynamics to intrinsic functional organization, we quantified regional homogeneity (ReHo) within the dmACC and

control-related networks, and examined how these ReHo measures related to metabolic responses and processing speed[39–43]. The older participants were included to extend the dynamic range of processing speed represented in the sample. Participants spanned overlapping ranges of cognitive performance across age groups, allowing us to examine metabolic responses across a broader spectrum of processing speed.

Based on previous fMRS studies reporting task-related increases in glutamate and lactate during sensory and cognitive stimulation [28,29,31,33–35,44–46], we hypothesized that cognitive engagement would increase both metabolites (Glutamate and Lactate) in the dmACC. We further examined whether individual differences in these neurochemical responses were associated with processing speed. Finally, we investigated whether local metabolic responses and processing speed were related to intrinsic regional and network-level functional organization.

Results

Participant characteristics

Twenty-six young adults (mean age, 26.00 ± 3.90 years) and eight older adults (75.40 ± 4.40 years) were included in the final fMRS sample. As expected, young and older participants differed in age ($t(32) = -33.80$, $p < 0.01$), while sex distribution was comparable across groups. Years of education did not differ significantly, although a trend toward more years of higher education was observed in the young group (Table 1).

All questionnaires and neuropsychological tests were completed before scanning. The DSST scores used in the correlation analyses were derived from the baseline paper-and-pencil Symbol Digit Substitution Test and were independent of performance on the verbal in-scanner symbol–digit matching task.

Behavioral measures confirmed a robust difference in processing speed between groups. Young participants outperformed older participants on the DSST ($t(32) = 6.10$, $p < 0.01$), consistent with preserved processing capacity in the younger cohort. Similarly, older participants showed significantly slower performance on the Trail Making Test, both for Part A ($t(32) = -5.00$, $p < 0.01$) and Part B ($t(32) = -3.90$, $p < 0.01$), indicating slower processing speed and executive-task performance. In contrast, Stroop task performance did not differ between groups for either congruent or incongruent conditions, suggesting that basic interference processing was relatively preserved (Table 1).

Global cognitive measures (MOCA) and additional behavioral indices (DMT, K10) did not show statistically significant group differences (Table 1).

Table 1 | Participant characteristics, data-quality measures, and cognitive performance.

Demographic characteristics, spectroscopy quality measures and cognitive performance are reported for younger and older participants. Values are mean ± SD unless otherwise indicated. DSST, Digit Symbol Substitution Test; TMT, Trail Making Test; MoCA, Montreal Cognitive Assessment; DMT, Digit Memory Test; K10, Kessler Psychological Distress Scale; FWHM, full width at half maximum. Higher DSST scores indicate better performance, whereas longer TMT completion times indicate poorer performance. Statistical comparisons and multiple-testing procedures are described in Methods.

Older adults show slower RT and reduced accuracy during in-scanner task

During the in-scanner task, older participants responded more slowly than younger participants in both conditions (control: young, 0.89 s; older, 1.60 s; stimulation: young, 1.37 s; older, 1.80 s; between-group contrasts, both $p < 0.01$; Fig. 1E). Within each group, reaction times increased during stimulation relative to control, reflecting the additional cognitive demands imposed by the paradigm.

Accuracy differed substantially between groups. While young participants performed near ceiling (95.06% [92.14, 97.98]), older participants showed markedly lower and more variable accuracy (70.13% [48.21, 92.04]). This indicates that, in addition to slower responses, older participants exhibited reduced task performance (Fig. 1E). The accuracy over the course of the experiment can be found in Supplementary Fig. 1. This performance difference is important when interpreting the metabolite results because the task may have imposed greater relative cognitive demand on the older group.

fMRI pilot localizer estimates

The spectroscopy voxel location was selected using an independent fMRI pilot localizer acquired in three participants. Each participant completed an extended block-design version of the task to obtain stable within-participant activation estimates. First-level activation maps for the task-versus-control contrast were combined using a fixed-effects analysis for descriptive localization only. Because the pilot sample was not intended to support population-level inference, the resulting map was used exclusively to guide voxel placement. Consistency of the activation location was additionally inspected across the three individual participant maps (Fig. 1C).

Metabolite dynamics and behavioral associations

We next examined task-related metabolite dynamics in the dmACC during cognitive engagement. Water linewidth (FWHM) did not differ significantly between groups ($t(32) = -2.00$, FDR-adjusted $p = 0.10$). Additional spectroscopy quality-control measures are reported in Supplementary Fig. 3.

Glutamate shows no reliable task-related modulation

Glutamate showed no significant modulation by task or age (condition: $F(1,381) = 0.65$, $p = 0.42$; age: $F(1,31.10) = 0.69$, $p = 0.41$). The age-by-condition interaction was also nonsignificant ($F(1,381) = 3.36$, $p = 0.07$, FDR-adjusted $p = 0.17$; Fig. 2A). Task-related glutamate change was not associated with baseline

DSST performance (r = 0.16, p = 0.40, FDR-adjusted p = 0.40; Fig. 2G). Associations with Trail Making performance were also nonsignificant (Supplementary Fig. 2).

Exploratory analyses of glutamate response timing used the 16-average time course (Supplementary Figs. 4–6). Glutamate increased from the last STIM average to the first subsequent CNTRL average in older adults (two-sided one-sample t test, unadjusted p < 0.01), whereas the corresponding test in younger adults was nonsignificant (p = 0.51; Supplementary Fig. 6C). The first and second CNTRL averages did not differ significantly in either group (young: p = 0.46; older: p = 0.99; Supplementary Fig. 6D). These within-group tests do not establish a between-group difference in response timing.

Lactate modulation and larger responses accompany slower processing speed

Lactate showed age-dependent task modulation. There were significant effects of age (F(1,28) = 15.14, p < 0.01) and condition (F(1,339) = 19.24, p < 0.01), together with an age-by-condition interaction (F(1,339) = 11.33, p < 0.01, FDR-adjusted p < 0.01; Fig. 2B). This interaction remained significant when the initial control block was included (F(1,394) = 10.34, FDR-adjusted p < 0.01).

Lactate concentrations were higher in older participants during both control (young: 0.95 [0.59, 1.31] mM; older: 2.09 [1.47, 2.71] mM; t(31.50) = − 3.25, p < 0.01) and stimulation (young: 0.99 [0.64, 1.35] mM; older: 2.44 [1.82, 3.06] mM; t(31.10) = − 4.12, p < 0.01). The stimulation-related increase was significant in older participants (0.35 mM, 95% CI [0.19, 0.50]; t(343) = 4.42, p < 0.01), whereas the corresponding contrast in younger participants was nonsignificant (p = 0.30).

Larger task-evoked lactate responses were associated with lower baseline DSST scores (r = − 0.56, 95% CI [− 0.78, − 0.22], n = 26; p < 0.01, FDR-adjusted p < 0.01; Fig. 2H). Supplementary analyses showed positive associations with TMT-A (r = 0.41, p = 0.04) and TMT-B completion time (r = 0.55, p < 0.01; Supplementary Fig. 2). Larger lactate responses thus accompanied slower performance across these measures.

The Glu/Lac ratio decreases with task engagement in older adults

The Glu/Lac ratio showed a significant age-by-condition interaction (F(1,317) = 6.71, p = 0.01, FDR-adjusted p = 0.03), with no significant main effect of age (F(1,27.29) = 2.91, p = 0.09) or condition (F(1,317) = 3.49, p = 0.06; Fig. 2C). The interaction was sensitive to inclusion of the initial control block (FDR-adjusted p = 0.21).

Estimated marginal means showed no significant between-group difference in Glu/Lac during CNTRL (young: 13.16, 95% CI [9.81, 16.51]; older: 9.49 [3.70, 15.27]; t(35.00) = 1.12, p = 0.27), but a higher ratio in younger participants during STIM (young: 13.71 [10.41, 17.01]; older: 6.10 [0.35, 11.85]; t(33.50) = 2.33, p = 0.02). Older participants showed a stimulation-related reduction (STIM − CNTRL: −3.39, 95% CI [− 6.00, − 0.77]; t(322) = − 2.55, p = 0.01), whereas the younger-group change was nonsignificant (p = 0.47). These contrasts exclude the first CNTRL block. The lower ratio during stimulation was observed alongside the lactate increase. The apparent rise during subsequent CNTRL blocks may suggest differences in relative

metabolite timing, but does not establish a delayed glutamate or oxidative response. Glu/Lac was treated as an exploratory measure of relative metabolite concentrations rather than a direct measure of metabolic flux.

Task-related Glu/Lac change was not associated with DSST performance ($r = 0.29$, $p = 0.15$, FDR-adjusted $p = 0.21$; Fig. 2I) or Trail Making performance (Supplementary Fig. 2).

ReHo is reduced with age across dmACC and control networks

We next examined whether intrinsic functional organization of the dmACC and associated large-scale networks relates to cognitive performance and neurochemical dynamics.

Regional homogeneity (ReHo) differed significantly between age groups across all regions of interest. Older participants showed reduced ReHo in the dmACC ($t(17.60) = 4.17$, $p < 0.01$), as well as in the executive ($t(24.70) = 6.34$, $p < 0.01$) and attention networks ($t(21) = 5.51$, $p < 0.01$), showing lower local functional coherence in the older group across the three prespecified regions/networks (Fig. 3A-C).

Lower ReHo accompanies larger task-evoked lactate responses

We next assessed whether resting-state organization relates to task-evoked neurochemical responses (Fig. 3D-I).

No significant associations were observed between task-related glutamate change and ReHo, either in the dmACC or at the network level (all $p \geq 0.33$), consistent with the absence of robust glutamate dynamics during task engagement.

In exploratory analyses using uncorrected p-values, larger lactate responses were associated with lower resting-state ReHo. Across participants, exploratory uncorrected correlations showed that greater task-related lactate increases were associated with lower ReHo in the dmACC ($r = -0.43$, $p = 0.04$), executive network ($r = -0.49$, $p = 0.02$), and attention network ($r = -0.43$, $p = 0.04$). These findings indicate that individuals with lower intrinsic functional coherence exhibit stronger glycolytic metabolic recruitment during cognitive engagement.

Higher ReHo accompanies faster processing speed

Across participants, exploratory uncorrected correlations showed that higher ReHo was associated with higher DSST scores (Fig. 3J–L): dmACC, $r = 0.44$, $p = 0.01$; executive network, $r = 0.50$, $p < 0.01$; and attention network, $r = 0.50$, $p < 0.01$.

These associations were not significant within either age group separately. Given the strong associations of age group with both ReHo and DSST performance, the combined-sample correlations cannot establish whether the relationships are continuous or primarily reflect between-group differences. These relationships across neurochemistry, intrinsic functional coherence, and cognitive performance are summarized in Fig. 4A and integrated conceptually in Fig. 4B.

Discussion

This study links processing speed to task-evoked metabolic responses in the dmACC and intrinsic network organization. Older participants showed larger lactate increases during cognitive engagement, and larger lactate responses were associated with lower DSST scores across all participants. Glutamate showed no significant group-level modulation, whereas the Glu/Lac ratio decreased during stimulation in older participants. Exploratory multimodal analyses further linked lower resting-state ReHo to both larger lactate responses and poorer processing speed. Together, these findings suggest that slower processing speed is accompanied by greater local metabolic recruitment and lower intrinsic network synchrony.

Efficient cognitive processing depends on tight coupling between neurotransmission and energy metabolism [17,19]. Glutamatergic signaling imposes substantial energetic demands, which are met through rapid metabolic adaptations, including glycolysis and lactate production [18,20]. Consistent with this framework, we observed task modulation of lactate, with a larger stimulation-related increase in older participants (during cognitive engagement), extending prior fMRS findings from sensory paradigms [45–47] to higher-order cognition [31,34]. Critically, these responses were not uniform across individuals but scaled with behavioral performance. This relationship suggests that the lactate response may index metabolic recruitment during cognitive engagement. Individuals with lower processing speed showed larger lactate changes. In contrast, more efficient individuals may operate closer to an optimal neuroenergetic regime, requiring less additional metabolic upregulation. The observed lactate–performance relationship can motivate a hypothesis about differing energetic support, but the present proton MRS data cannot determine whether oxidative metabolism was insufficient/inefficient or whether lactate provided an alternative energy source.

These findings align with emerging views that lactate plays an active role in supporting neuronal function and plasticity, rather than serving solely as a byproduct of metabolism [20,48]. Within this context, lactate dynamics provide a measurable index of the metabolic cost of cognition. Functional MRS studies have predominantly investigated visual and motor paradigms, where lactate increases of approximately 15–30% (and up to ~ 70% depending on acquisition and paradigm) represent the most robust metabolic response. A recent meta-analysis of 24 fMRS studies estimated a pooled task-related lactate increase of 22.2% (95% CI, 18.7–25.7%), with substantial between-study heterogeneity (I^2 = 74%)[32]. Glutamate/Glx increases accompany these changes with modest increases of around 2–10% and highly variable GABA changes [29,44–46]. In contrast, studies examining higher-order cognitive functions such as working memory, executive control, and learning have focused primarily on glutamate and GABA, typically reporting glutamate increases of only 2–12%, while dynamic lactate responses have rarely been investigated [29,31,49,50]. Our findings, therefore, extend the current fMRS literature by demonstrating that age-dependent lactate responses during higher-order cognition are measurable, exhibit larger task-related changes than other metabolites, and are associated with individual cognitive performance[29]. Caddye et al. (2026)[51] recently reported larger dACC lactate responses with increasing age during graded cognitive-emotional engagement, providing convergent evidence for age-dependent metabolic

recruitment. Our study extends this work to processing speed, linking larger task-related lactate responses to poorer DSST performance and, in exploratory analyses, lower resting-state regional homogeneity.

In contrast to lactate, glutamate did not show robust task-related modulation at the group level. Although previous fMRS studies have reported modest glutamate or Glx increases during sensory stimulation and cognitive paradigms such as working memory, executive control, and learning in the prefrontal cortex[31,34], these responses are generally smaller than lactate changes and exhibit substantially greater heterogeneity. Indeed, a recent meta-analysis reported only a modest overall effect for glutamate during cognitive paradigms, whereas GABA responses remained highly variable across studies, likely reflecting differences in task demands, brain region, experimental design, and acquisition methodology[35].

The magnitude of the expected response is important for interpreting the null group-level glutamate result. As summarized above, reported glutamate changes during cognitive tasks are typically only 2–12%, compared with lactate increases commonly around 15–30%. Against the relatively high baseline glutamate concentration in the dmACC, these smaller relative changes are harder to resolve. Between-participant differences in response timing, magnitude and potentially direction may further attenuate condition-averaged effects, particularly with limited signal-to-noise ratio and temporal averaging. These considerations leave open the possibility of transient physiological responses, although limited sensitivity cannot by itself explain the null result. Importantly, we observed trend-level age-dependent baseline differences, consistent with prior reports of reduced baseline glutamate in aging, particularly in the ACC [52].

The 16-average analysis provided finer temporal sampling than the primary condition comparison (Supplementary Fig. 4). Lactate showed larger excursions, whereas glutamate changes were smaller and less consistently task-locked. This difference is consistent with the relative response magnitudes reported in the literature and illustrates how temporal averaging may obscure heterogeneous glutamate responses. Exploratory analyses therefore examined peak amplitude, first-versus-second-average peak position within STIM, and residual deviation in the subsequent CNTRL period (Supplementary Fig. 5). None was significantly associated with DSST performance: peak amplitude, $r = 0.16$, $p = 0.40$; subsequent CNTRL deviation, $r = 0.05$, $p = 0.80$; and within-STIM peak position, Spearman $\rho = 0.28$, $p = 0.15$. Peak position was a coarse measure and did not estimate response onset or precise latency. These analyses address performance associations, whereas the transition analysis below tests whether glutamate continued to rise after STIM.

The Glu/Lac ratio decreased during stimulation in older participants but remained relatively stable in younger participants, consistent with the age-by-condition interaction. This interaction was sensitive to inclusion of the initial control block. The exploratory transition analysis showed a continued glutamate increase after STIM in older adults, consistent with a delayed or sustained response to cognitive engagement (Supplementary Fig. 6). The absence of a subsequent decline provides no evidence for a transient peak confined to the first CNTRL average. With 64-s spectral averages, these contrasts cannot

distinguish delayed response onset from continued accumulation or slow recovery. Glu/Lac describes the relative responses of the two metabolites rather than directly measuring oxidative and glycolytic flux. Whether response timing is associated with processing speed remains an open question. Prior carbon-13 MRS work supports coupling between neurotransmission and oxidative metabolism, providing physiological context for this interpretation; our glutamate concentration time course does not itself quantify oxidative flux or establish a delayed oxidative response [53,54].

A central contribution of this study is the integration of local neurochemical dynamics with intrinsic functional organization. While functional MRS captures metabolic responses within a localized cortical region, cognitive performance emerges from coordinated interactions across distributed brain network [2]. The present findings suggest that these two levels of organization are closely linked.

The dorsal (medial) anterior cingulate cortex (d(m)ACC), from which our spectroscopic measurements were obtained, occupies a central position within the brain's cognitive control architecture. It is a core node of the salience network and maintains dense connections with executive-control, attentional, and sensorimotor systems, enabling the integration of internal goals with external demands and the allocation of cognitive resources [41,42]. As such, the dACC has been proposed to act as a hub that coordinates transitions between large-scale brain networks during cognitively demanding behavior.

Consistent with this framework, we found that higher resting-state regional homogeneity (ReHo) within the dmACC and related control networks was associated with better processing speed, in agreement with previous work linking stronger local functional coherence to more efficient cognitive performance [9,11]. Importantly, these same ReHo measures were inversely associated with task-evoked lactate responses measured directly within the dmACC (Fig. 3E, G, I).

This inverse relationship suggests that intrinsic network organization influences the metabolic cost of cognitive processing. Individuals with lower resting-state functional coherence showed larger lactate increases during task performance, consistent with greater metabolic recruitment; however, differences in task performance preclude assuming equivalent cognitive demand across individuals. The fixed task may have imposed greater relative cognitive demand on older participants, as suggested by their slower responses and lower accuracy. Larger lactate responses could therefore reflect greater metabolic recruitment at a higher relative workload, rather than an age-specific metabolic alteration alone. Future studies using graded or individually calibrated task difficulty could distinguish responses to a common external demand from differences that persist at comparable relative workloads. Conversely, stronger intrinsic organization may enable the dmACC to coordinate information processing more efficiently across distributed networks, thereby reducing local metabolic requirements.

Although the present data are correlational, they support the hypothesis that the dACC links systems-level network organization with cellular energy metabolism. Rather than reflecting independent phenomena, intrinsic functional architecture and task-related neuroenergetic responses appear to represent complementary aspects of the same neural infrastructure supporting cognitive efficiency [43].

This interpretation is consistent with models that view the dACC as a central hub for allocating cognitive resources, monitoring behavioral demands, and orchestrating interactions between salience and executive-control networks during goal-directed behavior [42]. The convergence of these relationships across intrinsic network organization, metabolic recruitment, and cognitive performance is summarized in Fig. 4A & B.

Cognitive challenges may reveal differences between preserved and impaired metabolic adaptation that are not fully captured by resting metabolite concentrations. Both the magnitude and slope of the metabolic response, interpreted alongside achieved performance, may help distinguish effective recruitment from emerging dysfunction. Such challenge-based measures could potentially identify metabolic vulnerability before overt cognitive or clinical symptoms emerge, a possibility that requires longitudinal validation.

Neuroenergetic flexibility may be defined as the capacity to match metabolic recruitment to cognitive demand while maintaining performance. A larger lactate response alone does not establish greater flexibility or compensation: it may reflect resource mobilization, higher relative workload, or greater energetic cost. Its functional benefit cannot be inferred from the observed correlation.

The combined-sample lactate–behavior and ReHo–behavior associations are compatible with a continuum across individuals, but the present sample cannot distinguish this interpretation from differences between the young and older groups. Aging may shift the operating point of this system: as intrinsic functional organization becomes less efficient and baseline metabolic conditions change, greater recruitment may be required at lower levels of cognitive demand, while the remaining capacity for further upregulation becomes progressively constrained. This interpretation parallels load-dependent models of cognitive aging, including the compensation-related utilization of neural circuits hypothesis, in which older adults recruit additional neural resources at relatively low task demands but reach their processing ceiling earlier as demands increase [55–58]. The present findings suggest that such shifts in functional recruitment may be accompanied by corresponding shifts in metabolic demand.

This continuum may extend beyond healthy aging. Reduced efficiency and compensatory over-recruitment have also been described in conditions characterized by cognitive slowing or impaired cognitive control, including schizophrenia, multiple sclerosis, and traumatic brain injury. In these conditions, relatively preserved performance can coexist with broader or stronger recruitment of control networks, particularly at lower task demands, whereas performance deteriorates once compensatory capacity is exhausted. Altered cerebral energy metabolism is additionally implicated in Alzheimer’s disease and related neurodegenerative processes, where glucose hypometabolism, mitochondrial dysfunction, and impaired metabolic support may restrict the energetic reserve available for adaptive recruitment. These observations raise the possibility that aging and disease differ partly in the extent to which the neuroenergetic system has shifted away from its efficient operating range, rather than in the presence of wholly distinct mechanisms [59–63].

Future studies should investigate this framework in populations with mild cognitive impairment (MCI), which represents a clinically relevant transitional stage between healthy aging and dementia and is characterized by early deficits in processing speed, executive function, and brain energy metabolism. Because functional MRS directly measures task-related neurochemical dynamics rather than relying on hemodynamic responses, it may provide a more specific assessment of neuronal metabolic function in aging populations, where neurovascular coupling becomes progressively disrupted, potentially reducing the interpretability of BOLD-fMRI as a direct surrogate of neuronal activity [64]. Combining fMRS-derived measures of neuroenergetic flexibility with functional network metrics may therefore offer a promising approach for identifying early metabolic dysfunction preceding overt neurodegeneration and for distinguishing impaired energetic adaptation from changes driven primarily by vascular dysfunction.

Several limitations should be considered. The older cohort was included to extend the range of processing speed rather than to characterize aging, and its small size limits population-level inference. Detecting the small relative glutamate responses discussed above against a high baseline concentration requires sufficient sample size, spectral sensitivity and temporal resolution. The block design may obscure transient or delayed responses, while fixed task difficulty may impose different relative workloads across participants. Resting-state and task-based measures were analyzed separately, and the correlational design cannot establish causal relationships between intrinsic organization, metabolic recruitment and performance.

Larger cohorts, graded task demands and finer temporal sampling are needed to distinguish response magnitude, onset, peak latency and recovery, and to test whether metabolic responses predict cognitive decline. Extending this approach to clinical populations will establish its translational relevance.

Conclusion

The present study links individual differences in processing speed to task-evoked neuroenergetic responses in the human dmACC. Larger lactate increases in individuals with poorer performance suggest greater recruitment of non-oxidative metabolism during cognitive demand, while associations with intrinsic functional organization place these local responses within a broader systems-level context. The differential modulation of lactate and glutamate, together with the age-dependent Glu/Lac response, further suggests an altered balance between oxidative and non-oxidative metabolism with aging. The exploratory post-task glutamate increase in older adults suggests that temporal dynamics may provide information beyond condition-averaged responses, whereas the magnitude of the lactate response was directly associated with individual cognitive performance. Together, these findings suggest that cognitive performance is related not only to the magnitude of local metabolic recruitment during task engagement, but also to the temporal balance between oxidative and non-oxidative metabolism and the intrinsic functional organization of brain networks. By directly measuring metabolic dynamics during cognition, fMRS provides information complementary to conventional functional neuroimaging and may be particularly valuable for investigating cognitive aging and conditions in which neurovascular coupling or cerebral metabolism is altered.

Methods

Participants and MR Scanning Protocol:

Participants were recruited through posters displayed at Campus Biotech and online advertisements distributed by the Fondation Campus Biotech Geneva (FCBG). Young adults were eligible if they were aged 18–30 years, and older adults if they were aged ≥ 65 years. All participants were required to be physically and psychologically healthy. Older participants were additionally screened for mild cognitive impairment using the Montreal Cognitive Assessment (MoCA). Exclusion criteria included contraindications to MRI.

A total of 30 young and 10 older adults were initially recruited. Four young participants were excluded because of insufficient spectral signal-to-noise ratio (SNR < 10) and quality measures, and the fMRS data of two older participants were unusable because of severe lipid contamination and baseline distortion. The final sample therefore comprised 26 young adults and eight older adults. Participant sex and further demographic characteristics are reported in Table 1.

The target sample size was determined based on effect sizes reported. The sample-size calculation was informed by prior fMRS work on age-related differences in glutamate responses during memory encoding[65]. Assuming an effect size of d = 0.95, 95% power and a two-sided α = 0.05, the planned comparison required 25 participants per group. The study design was subsequently revised to retain a target of 30 younger participants (to account for drop-out) and include a smaller, exploratory older arm to extend the range of processing speed. The older arm was therefore not powered to be exploratory. All participants received written information about the study and provided written informed consent before participation. The study was conducted in accordance with the Declaration of Helsinki and was approved by the cantonal ethics committees of Vaud and Geneva, Switzerland (BASEC-2023-00370). Participants received CHF 50 as compensation for their participation.

Participants underwent 7T MR scanning on a Siemens Terra.X system (Siemens Medical Solutions, Erlangen, Germany) equipped with a 32-channel NOVA head coil. The older participants were included to extend the range of processing speed rather than to characterize ageing.

Participants arrived approximately one hour prior to MRI acquisition. During this time, the experimental procedures were explained in detail, and participants practiced the Symbol Digit Matching Task (SDMT) using a paper-based example to ensure full comprehension of the task demands.

Prior to scanning, participants completed a cognitive and behavioral assessment battery including:

- Montreal Cognitive Assessment (MoCA) [66]
- Kessler Psychological Distress Scale (K10) [67]
- Trail Making Test (Parts A and B) [68]
- Stroop Task [69]

- Digit Symbol Substitution Test (DSST) [70]
- Digit Memory Task [71]

Demographic information was collected, including age and years of education (separately documented for pre-higher education and higher education).

MRI sessions included high-resolution structural imaging for voxel placement and anatomical reference, as well as functional ^{1}H MRS acquisition during the SDMT paradigm to assess dynamic metabolite changes.

Task Design and Procedure:

Participants performed a Symbol Digit Matching Task (SDMT) [72] during continuous 7 T proton functional magnetic resonance spectroscopy (^{1}H-fMRS; Fig. 1B). Before scanning, participants received standardized instructions and practised the task outside the scanner using a paper-based version to ensure that they understood the symbol–digit mapping and verbal-response requirements.

The experiment comprised eight alternating 128-s blocks: four digit-reading control blocks and four active symbol–digit matching blocks, presented in the fixed order control–stimulation, repeated four times. Each block contained 64 trials presented at 2-s intervals. Stimuli were presented using PsychoPy 2023.1.2.

During active blocks, a symbol–digit key was displayed at the top of the screen (Fig. 1B). On each trial, participants verbally reported the digit corresponding to the presented symbol. To limit learning and memorization, the symbol–digit key was replaced every 32s within each active block. During control blocks, participants read aloud single digits presented with the same trial timing. This condition was designed to account for visual stimulation and speech production while minimizing symbol–digit matching and associated cognitive demands. Verbal responses were recorded using an MR-compatible noise-cancelling microphone and subsequently used to calculate response accuracy and reaction time, as described under Behavioral Analysis.

Behavioral Data Processing

Verbal responses and task-timing signals were recorded on separate audio channels and processed offline. The recordings were denoised and temporally aligned using peaks detected in the task-timing signal. Verbal-response onsets were identified from the participant audio, and reaction time was defined as the interval between the corresponding task signal and the onset of the verbal response.

Reaction-time series were inspected for detection artefacts. Values between 0 and 0.60 s, as well as values exceeding 2s when followed by a zero-valued observation, were identified as artefactual and replaced with the mean of the neighboring observations. Additional outliers exceeding three standard deviations from a centered 10-trial rolling mean were identified and replaced in the same manner. Mean

reaction time was then calculated across the 64 trials within each of the eight blocks. Block-averaged reaction times were used to summarize participant performance; age and condition effects were assessed using the finer-grained reaction-time observations.

Spoken digits were initially identified using automated speech recognition and subsequently verified manually against the audio recordings. The verified responses were compared with the correct responses reconstructed from the symbol–digit mappings recorded by the task software. Responses were scored as correct or incorrect, with missing responses classified as incorrect. Accuracy was calculated separately for each of the four task blocks as the percentage of correct responses across 64 trials; overall accuracy was calculated across all 256 task trials.

Scores from the Montreal Cognitive Assessment (MoCA), Kessler Psychological Distress Scale (K10), Trail Making Test parts A and B, Stroop task, Digit Symbol Substitution Test (DSST), and Digit Memory Task were calculated according to their respective standardized scoring procedures. The DSST was the primary out-of-scanner measure of processing speed. TMT-A and TMT-B completion times and the remaining cognitive measures were included for participant characterization and exploratory analyses (Supplementary Materials & Results).

MRI Acquisition Protocol

All MRI data were acquired on a 7T Siemens MAGNETOM Terra.X system (Siemens Healthineers, Erlangen, Germany; syngo MR XA60) at Fondation Campus Biotech (Geneva, Switzerland), using an 8Tx/32Rx NOVA head coil. Participants were positioned head-first supine and stabilized using foam padding to minimize motion.

First, high-resolution structural images were acquired using a 3D MP2RAGE sequence (0.66 mm isotropic resolution; TR = 6 s; TE = 3.08 ms). The resulting T1-weighted images and quantitative T1 maps were used for anatomical reference, spectroscopy voxel planning in the dorsal medial anterior cingulate cortex (dmACC), and subsequent spatial registration.

Following anatomical acquisition, a B1 + transmit field map was obtained using a 2D gradient-recalled flip-angle mapping sequence (TR = 4 s; TE = 1.73 ms; flip angle = 5°; slice thickness = 4 mm; matrix = 64 × 64; parallel imaging factor = 2). The B1 + map was used to assess transmit field homogeneity and to optimize RF amplitude calibration prior to spectroscopy.

A 20×20×25-mm³ spectroscopy voxel was positioned manually in the dorsal medial anterior cingulate cortex (dmACC; Fig. 1C). Placement was guided by the anterior commissure–posterior commissure plane and consistent anatomical landmarks: the voxel was positioned approximately one sulcus superior to the corpus callosum and one sulcus anterior to the motor cortex, with its orientation aligned with the brainstem.

B0 homogeneity within the voxel was optimized using the vendor-provided shimming procedure. An unsuppressed water spectrum was subsequently acquired, and shimming was repeated when the water

linewidth exceeded 17 Hz. Once a water linewidth below 17 Hz had been achieved, a short test acquisition comprising eight spectral averages was visually inspected for adequate spectral quality before the functional acquisition was initiated. Water-reference linewidths are reported in Table 1, and blockwise linewidth, signal-to-noise ratio and metabolite-fitting uncertainty are reported in Supplementary Fig. 3.

Localized 1H-MR spectra were acquired using semi-adiabatic spin-echo full-intensity-acquired localization (sSPECIAL) techniques with the following parameters: TR/TE = 4000/16 ms, bandwidth = 4 kHz, and 4096 data points per spectrum, voxel size = 20 × 20 × 25 mm^3 (Fig. 1C). Each 128-s block corresponded to 32 spectral averages (TR = 4 s), resulting in four control and four stimulation spectra per participant for blockwise metabolite quantification.

After completion of the spectroscopy protocol, a resting-state functional MRI scan was collected using a multiband gradient-echo EPI sequence (1.30 mm isotropic resolution; TR = 1.55 s; TE = 26 ms; flip angle = 63°; multiband factor = 3; total readout time = 36.24 ms; phase-encoding direction j−; 250 volumes, plus 2 non-steady-state). The run comprised 250 analyzed volumes preceded by two non-steady-state volumes and lasted approximately 6 min 28 s. Participants were instructed to look at a fixation cross in the center of the screen, keep their eyes open, remain awake and allow their minds to wander. Wakefulness was not monitored objectively. An additional spin-echo EPI acquisition with reversed phase encoding was collected for susceptibility-distortion correction.

MRI pre-processing

Structural and resting-state functional MRI data were preprocessed using *fMRIPrep* 25.1.4 (RRID:SCR_016216), which is based on *Nipype* 1.10.0 (RRID:SCR_002502), and applied to BIDS-formatted data.

Anatomical Data

The T1-weighted MP2RAGE image was first corrected for intensity non-uniformity using N4BiasFieldCorrection (ANTs 2.3.4), skull-stripped using an ANTs-based brain extraction workflow, and segmented into cerebrospinal fluid (CSF), white matter (WM), and gray matter (GM) using FSL FAST. Cortical surfaces were reconstructed with FreeSurfer (recon-all). The anatomical image was then nonlinearly normalized to MNI152NLin2009cAsym standard space using ANTs (antsRegistration), with templates accessed via TemplateFlow.

Functional MRI data

For the resting-state EPI run, preprocessing included susceptibility distortion correction using a reversed phase-encoding acquisition and FSL topup, followed by head-motion correction using MCFLIRT. The functional data were co-registered to the anatomical reference using boundary-based registration and subsequently resampled using a single interpolation step that combined motion correction, distortion

correction, and spatial normalization. Volumetric resampling was performed using cubic B-spline interpolation.

Framewise displacement, standardized DVARS and motion-outlier indicators were calculated during fMRIPrep preprocessing and exported with the confounds files. XCP-D applied a 36-parameter nuisance-regression model comprising six rigid-body motion parameters and mean global, white-matter and cerebrospinal-fluid signals, together with their temporal derivatives and quadratic expansions. The complete autogenerated fMRIPrep boilerplate text is provided in the Supplementary Material.

Functional MR Spectroscopy Data

Spectral preprocessing was performed using MRSpecLAB[73], our in-house processing platform. Individual free induction decays were first coil-combined using complex-weighted summation, followed by frequency and phase alignment to correct for temporal drift. Eddy-current correction was applied using the unsuppressed water reference acquired prior to the functional run. Spectra were then averaged according to predefined analysis schemes and exported for quantification with LCModel (Fig. 1D).

All spectra were visually inspected both transient-by-transient and after averaging to ensure spectral stability and minimal phase inconsistencies between averages. Particular attention was given to the presence and stability of low-concentration metabolites. All spectra were visually inspected for spectral stability and phase consistency. Block-wise quality-control measures, including linewidth, signal-to-noise ratio, and fitting uncertainty for glutamate and lactate, are reported in Supplementary Fig. 3.

To investigate dynamic metabolite changes, several averaging strategies were implemented: (i) full-condition averaging (all control vs. all stimulation blocks), (ii) block-wise averaging (one spectrum per 128 s block), and (iii) sub-block averaging (two spectra per block). This approach allowed evaluation of both condition-level effects and temporal dynamics across the task.

Metabolite concentrations were quantified relative to the unsuppressed water signal. LCModel fitting used a basis set, containing 21 metabolite components and an explicit macromolecular component. Spectra were fitted over 0.20–4.20 ppm, with an echo time of 16.00 ms, 4096 data points and an acquisition dwell time of 125 µs. Water scaling was enabled using the corresponding unsuppressed water reference. The complete control-file settings and basis-set composition are provided in the Supplementary Methods. Analyses focused on N-acetylaspartate (NAA), total creatine (tCr), glutamate (Glu), lactate (Lac), and glutathione (GSH). LCModel control files, basis set specifications, and fitting parameters are provided in the Supplementary Material in accordance with MRSinMRS reporting guidelines.

Spectral quality was assessed using visual inspection, signal-to-noise ratio, linewidth and LCModel fitting uncertainty. No additional numerical SNR or linewidth exclusion threshold was applied. Metabolite-specific participant exclusions and selected lactate omissions are detailed in Supplementary Methods. Participant-number exclusions were based on visual inspection of spectral quality.

To account for partial volume effects, metabolite concentrations were corrected for tissue composition using gray matter (GM), white matter (WM), and cerebrospinal fluid (CSF) fractions derived from segmentation of the MP2RAGE anatomical image during fMRIPrep preprocessing. Tissue correction followed standard approaches assuming negligible metabolite contribution from CSF and adjusting water scaling accordingly.

Resting-State fMRI Post-processing and Analysis

Post-processing of the fMRIPrep outputs was performed using the eXtensible Connectivity Pipeline–DCAN (XCP-D; version 0.11.2.dev2 + g402269a) in LINC mode. Denoising used the 36P strategy, comprising the six rigid-body motion parameters and mean global, white-matter and cerebrospinal-fluid signals, together with their temporal derivatives and quadratic expansions. BOLD data were despiked using AFNI's 3dDespike. The BOLD time series and nuisance regressors were band-pass filtered between 0.01 and 0.08 Hz using a second-order Butterworth filter before nuisance regression. The XCP-D temporal masks contained zero censored resting-state volumes in both age groups. No participant was excluded because of rs-fMRI quality, and one participant did not undergo rs-fMRI acquisition. A separate denoised BOLD derivative was spatially smoothed using Connectome Workbench with a 6-mm full-width-at-half-maximum Gaussian kernel.

Cortical ReHo was calculated from the temporally filtered, denoised, unsmoothed functional data separately for each hemisphere using surface-based 2dReHo. Kendall's coefficient of concordance was calculated between each surface vertex and its nearest-neighbour vertices. Subcortical ReHo was calculated using AFNI's 3dReHo. ReHo values were retained as native Kendall's coefficients of concordance without whole-brain normalization, and the ReHo maps were not spatially smoothed.

XCP-D also generated atlas-based functional-connectivity matrices as routine pipeline outputs. The analyses reported here focused on ReHo in the dmACC and the executive and attention network composites.

The complete autogenerated XCP-D boilerplate text is provided in the Supplementary Material.

Definition of regions of interest and functional networks

The dmACC region of interest was defined as a bilateral composite of Glasser atlas areas 7AL and 8BM (Right_7AL, Right_8BM, Left_7AL and Left_8BM). The spatial correspondence between this region and the MRS voxel location is shown in the left panel of Fig. 3. This definition captures a dorsal medial prefrontal region overlapping with the MRS voxel and provides anatomically specific coverage of the dmACC, a region consistently implicated in cognitive control, performance monitoring, and effort allocation.

To characterize intrinsic functional organization, regional homogeneity (ReHo) was used as a measure of local functional coherence, reflecting the similarity of the time series of a given voxel or parcel with its

neighbors. ReHo was selected as a robust, model-free index of local synchronization, well suited to capture baseline functional architecture and previously linked to cognitive performance and capacity.

Network-level measures were derived using the Gordon atlas. Rather than relying on single predefined networks, composite measures were constructed a priori to capture broader functional systems. The executive network was defined as the combination of FrontoParietal and CinguloOpercular parcels, reflecting distributed control-related processes. The attention network was defined as the combination of DorsalAttn and VentralAttn parcels, capturing both goal-directed and stimulus-driven attentional systems. Network-level ReHo values were computed as the unweighted mean of the parcel-level ReHo values across all parcels belonging to each composite network. This multiscale approach, combining a targeted dmACC definition with both local (ReHo) and network-level functional metrics, enabled the integration of neurochemical measurements with intrinsic functional organization across spatial scales.

Statistical Analysis

Statistical analyses were performed in R version 4.4.0. Continuous variables are reported as means with standard deviations or 95% confidence intervals, as indicated. Demographic, neuropsychological, and data-quality measures were compared between young and older adults using two-sample Welch's t-tests or non-parametric tests when distributional assumptions were not met. In-scanner task accuracy was compared between age groups using Welch's two-sample t-test.

Individual reaction-time observations were analyzed using a linear mixed-effects model with task condition, age group, and their interaction as fixed effects and participant as a random intercept. Post hoc contrasts estimated between-group differences within each condition and within-group differences between conditions.

Glutamate, lactate and the Glu/Lac ratio were analysed separately using linear mixed-effects models fitted to the original measured values. The condition models included task condition (CNTRL versus STIM), age group, their interaction, centred linear block order (block number − 4.50), and the age-by-time interaction as fixed effects, with participant as a random intercept. These models estimated condition effects while allowing different linear time trends between age groups. The condition comparison in panels A–C excluded the first CNTRL block; analyses accompanying panels D–F used all eight blocks. The initial control period was excluded because anticipatory arousal and adaptation to the experimental setting may make it less representative of subsequent control periods. This rationale is consistent with prior fMRS work selecting later portions of stimulation and subsequent rest periods to avoid transient metabolic effects[28]. Analyses including the initial control block assessed sensitivity to this choice. Within-age condition effects across all blocks were tested using models containing condition and linear time as fixed effects and participant as a random intercept. Models were fitted by maximum likelihood; omnibus effects were evaluated using F-tests with Satterthwaite degrees of freedom, and estimated marginal-means contrasts used FDR adjustment. A separate exploratory model included eight-level categorical block, age group and their interaction. This categorical-block model was fitted to unadjusted

values because a linear time term cannot be independently identified alongside all eight block levels. Detrended values were used for the main figure display, whereas condition-model inference used the original observations with time included explicitly.

For visualization and participant-level DSST analyses, linear time trends were estimated separately for each participant and measure by ordinary least-squares regression of the measured value on condition (CNTRL = 0, STIM = 1) and centred block order (block number − 4.50). Only the fitted linear time component was subtracted from each observation, retaining the fitted condition effect and residual variation. The Glu/Lac ratio was calculated from paired concentrations at each time point and detrended directly. Task-related responses were calculated as Δ% = 100 × (mean detrended STIM − mean detrended CNTRL)/mean detrended CNTRL. Pearson correlations assessed their associations with pre-scan DSST scores across participants. These correlations were considered exploratory and represent a two-stage analysis that does not propagate uncertainty in the participant-specific trend estimates. Associations between ReHo and metabolite responses used the same detrended participant-level percentage changes as the DSST analyses. Supplementary TMT correlations used the original, unadjusted condition-averaged responses. Unadjusted metabolite analyses were retained for comparison.

Exploratory post-stimulation glutamate dynamics were assessed using the 16-average data after participant-specific linear detrending (Supplementary Fig. 6). For each available STIM-to-CNTRL transition (averages 4–5, 8–9 and 12–13), we calculated first CNTRL minus last STIM and first CNTRL minus second CNTRL. Each spectral average spanned 64 s. Available paired contrasts were averaged within each participant, and these participant means were tested against zero separately within each age group using two-sided one-sample t tests, without multiple-comparison correction. Missing pairs were omitted without imputation. Group means and 95% confidence intervals were calculated from the participant mean contrasts. Profile plots used complete three-position transitions, so their contributing observations could differ from those of the contrast tests.

Resting-state regional homogeneity was compared between age groups using two-sample Welch's t-tests. Pearson correlations were used to examine associations of ReHo with processing speed and task-related metabolite responses across the combined sample. These multimodal correlations were considered exploratory.

For each metabolite measure, Benjamini–Hochberg false discovery rate correction was applied across three displayed tests: the age-by-condition interaction after excluding the first CNTRL block, the age-by-condition interaction using all eight blocks, and the association between detrended task-related percentage change and DSST score. The second test assesses condition modulation across the full acquisition; it is distinct from the age-by-block interaction in the exploratory eight-level block model. Uncorrected and FDR-adjusted p-values are reported where applicable. Exploratory within-age condition tests and eight-block time-course analyses are reported with uncorrected omnibus p-values; estimated marginal-means contrasts were adjusted as specified above. The rs-fMRI analyses remained exploratory. All tests were two-sided with $\alpha = 0.05$.

Declarations

Competing interests

The authors declare no competing interests.

Author contributions

A.K.: Conceptualization, Methodology, Investigation, Formal analysis, Data curation, Visualization, Project administration, Writing – original draft, Writing – review & editing. Y.X.: Methodology, Software, Validation, Writing – review & editing. I.K.: Investigation, Resources, Writing – review & editing. M.W., Y.L., D.W., and D.K.: Writing – review & editing. K.Q.D.: Writing – review & editing. L.X.: Conceptualization, Funding acquisition, Resources, Supervision, Writing – review & editing. All authors read and approved the final manuscript.

Acknowledgements

We thank all participants who took part in this study. We thank Nathalie Philippe and Loan Mattera for their assistance with participant recruitment and the students who contributed to data acquisition and analysis, particularly Nico Valsangiacomo and Mischa Mez. We acknowledge the MRI Platform of the Fondation Campus Biotech Geneva (FCBG) and the CIBM Center for Biomedical Imaging for providing the expertise and resources required to conduct this study. This work was supported by the Swiss National Science Foundation (SNSF Consolidator Grant #213769).

Data availability

The data supporting the findings of this study are available from the corresponding author upon reasonable request. Individual-level data are not publicly available because they contain information that could compromise participant privacy and are subject to the conditions of the ethical approval and informed consent.

Code availability

Spectroscopy data were processed using MRSpecLAB, which is openly available at https://github.com/MRSEPFL/MRspecLAB. MRI data were processed using the standardized open-source pipelines fMRIPrep (https://github.com/nipreps/fmriprep) and XCP-D (https://github.com/PennLINC/xcp_d). Study-specific scripts used for statistical analysis and figure generation are available from the corresponding author upon reasonable request.

References

1. Buzi G, Eustache F, Droit-Volet S, Desaunay P, Hinault T (2024) Towards a neurodevelopmental cognitive perspective of temporal processing. Commun Biol 7:987
2. Duncan J, Assem M, Shashidhara! S (2020) Integrated intelligence from distributed brain activity. Trends Cogn Sci 24:838–852
3. Eckert MA (2011) Slowing Down: Age-Related Neurobiological Predictors of Processing Speed. Front Neurosci 5:25
4. Haran JP et al (2025) Executive functioning and processing speed as predictors of global cognitive decline in Alzheimer's disease. J Alzheimers Dis Rep 9:25424823251363549
5. Ebaid D, Crewther SG (2020) Time for a Systems Biological Approach to Cognitive Aging?—A Critical Review. Front Aging Neurosci 12
6. Wang Y-TL, Zhang C,Jia-Cheng Han,Yu-Xuan Shang,Zhu-Hong Chen,Guang-Bin Cui,Wen. Neuroimaging features of cognitive impairments in schizophrenia and major depressive disorder - Yu-Ting Li, Zhang C, Han J-C, Shang Y-X, Chen Z-H, Cui G-B (2024) Wen Wang, *Ther. Adv. Psychopharmacol.* https://journals.sagepub.com/doi/10.1177/20451253241243290 (2024)
7. Mathias SR et al (2017) The Processing-Speed Impairment in Psychosis Is More Than Just Accelerated Aging. Schizophr Bull 43:814–823
8. McCutcheon RA, Keefe RSE, McGuire PK (2023) Cognitive impairment in schizophrenia: aetiology, pathophysiology, and treatment. Mol Psychiatry 28:1902–1918
9. Argyelan M et al (2015) Abnormal Resting State fMRI Activity Predicts Processing Speed Deficits in First-Episode Psychosis. Neuropsychopharmacology 40:1631–1639
10. Carter SL et al (2023) Differences in resting state functional connectivity relative to multiple sclerosis and impaired information processing speed. Front Neurol 14
11. Liégeois R et al (2019) Resting brain dynamics at different timescales capture distinct aspects of human behavior. Nat Commun 10:2317
12. Nolin SA et al (2025) Network segregation is associated with processing speed in the cognitively healthy oldest-old. eLife 14:e78076
13. Northoff G (2024) Beyond mood — depression as a speed disorder: biomarkers for abnormal slowness. J Psychiatry Neurosci JPN 49:E357–E366
14. Salthouse TA (2000) Aging and measures of processing speed. Biol Psychol 54:35–54
15. Deary IJ, Penke L, Johnson W (2010) The neuroscience of human intelligence differences. Nat Rev Neurosci 11:201–211
16. Penke L et al (2010) A General Factor of Brain White Matter Integrity Predicts Information Processing Speed in Healthy Older People. J Neurosci 30:7569–7574
17. Attwell D, Laughlin SB (2001) An Energy Budget for Signaling in the Grey Matter of the Brain. J Cereb Blood Flow Metab 21:1133–1145

18. Dienel GA (2012) Brain lactate metabolism: the discoveries and the controversies. J Cereb Blood Flow Metab 32:1107–1138
19. Harris JJ, Jolivet R, Attwell D (2012) Synaptic Energy Use and Supply. Neuron 75:762–777
20. Magistretti PJ, Allaman I (2018) Lactate in the brain: from metabolic end-product to signalling molecule. Nat Rev Neurosci 19:235–249
21. Vaccari-Cardoso B, Antipina M, Teschemacher AG, Kasparov S (2022) Lactate-Mediated Signaling in the Brain—An Update. Brain Sci 13:49
22. Zhang S et al (2026) From energy metabolism to mood regulation: The rise of lactate as a therapeutic target. J Adv Res 80:535–554
23. Schaller B, Xin L, O'Brien K, Magill AW, Gruetter R (2014) Are glutamate and lactate increases ubiquitous to physiological activation? A 1H functional MR spectroscopy study during motor activation in human brain at 7 Tesla. *NeuroImage* 93, 138–145
24. Yang W, Xu Y, Wang K (2026) Lactate and cognition: a dual modulator. Front Mol Neurosci 19:1742681
25. Chen R et al (2025) MRS Perspectives: Neurotransmitter and Metabolic Alterations in Cognitive Decline and Mental/Neurological Disorders. https://doi.org/10.2174/011570159X402624250926110831 doi:10.2174/011570159X402624250926110831
26. Stanley JA, Raz N (2018) Functional Magnetic Resonance Spectroscopy: The New MRS for Cognitive Neuroscience and Psychiatry Research. Front Psychiatry 9
27. Mullins PG (2018) Towards a theory of functional magnetic resonance spectroscopy (fMRS): A meta-analysis and discussion of using MRS to measure changes in neurotransmitters in real time. Scand J Psychol 59:91–103
28. Bednařík P et al (2015) Neurochemical and BOLD responses during neuronal activation measured in the human visual cortex at 7 Tesla. J Cereb Blood Flow Metab 35:601–610
29. Koush Y, Rothman DL, Behar KL, de Graaf RA, Hyder F (2022) Human brain functional MRS reveals interplay of metabolites implicated in neurotransmission and neuroenergetics. J Cereb Blood Flow Metab 42:911–934
30. Lynn J, Woodcock EA, Anand C, Khatib D, Stanley JA (2018) Differences in steady-state glutamate levels and variability between 'non-task-active' conditions: Evidence from 1H fMRS of the prefrontal cortex. NeuroImage 172:554–561
31. Woodcock EA, Anand C, Khatib D, Diwadkar VA, Stanley JA (2018) Working Memory Modulates Glutamate Levels in the Dorsolateral Prefrontal Cortex during 1H fMRS. Front Psychiatry 9:66
32. Cairone L, Guidi M, Mancini M, Giove F (2026) Lactate Changes Quantified by fMRS: A Meta-Analysis. NMR Biomed 39:e70295
33. DiNuzzo M et al (2022) Perception is associated with the brain's metabolic response to sensory stimulation. eLife 11:e71016

34. Lynn J, Woodcock EA, Anand C, Khatib D, Stanley JA (2018) Differences in steady-state glutamate levels and variability between 'non-task-active' conditions: Evidence from 1H fMRS of the prefrontal cortex. NeuroImage 172:554–561
35. Pasanta D et al (2023) Functional MRS studies of GABA and glutamate/Glx – A systematic review and meta-analysis. Neurosci Biobehav Rev 144:104940
36. Nee DE, Kastner S, Brown JW (2011) Functional heterogeneity of conflict, error, task-switching, and unexpectedness effects within medial prefrontal cortex. NeuroImage 54:528–540
37. Friedman NP, Robbins TW (2022) The role of prefrontal cortex in cognitive control and executive function. Neuropsychopharmacology 47:72–89
38. Shenhav A, Botvinick MM, Cohen JD (2013) The expected value of control: An integrative theory of anterior cingulate cortex function. Neuron 79:217–240
39. Geng H, Xu P, Aleman A, Qin S, Luo Y-J (2024) Dynamic Organization of Large-scale Functional Brain Networks Supports Interactions Between Emotion and Executive Control. Neurosci Bull 40:981–991
40. Stein J, Korb FM, Goschke T, Zwosta K (2025) Salience network resting-state functional connectivity predicts self-controlled decision-making. Sci Rep 15:16332
41. Gratton C, Sun H, Petersen SE (2018) Control networks and hubs. Psychophysiology 55:e13032
42. Seeley WW et al (2007) Dissociable Intrinsic Connectivity Networks for Salience Processing and Executive Control. J Neurosci 27:2349–2356
43. Ham T, Leff A, de Boissezon X, Joffe A, Sharp DJ (2013) Cognitive Control and the Salience Network: An Investigation of Error Processing and Effective Connectivity. J Neurosci 33:7091–7098
44. Boillat Y, Xin L, Van Der Zwaag W, Gruetter R (2020) Metabolite concentration changes associated with positive and negative BOLD responses in the human visual cortex: A functional MRS study at 7 Tesla. J Cereb Blood Flow Metab 40:488–500
45. Mangia S et al (2007) Dynamics of lactate concentration and blood oxygen level-dependent effect in the human visual cortex during repeated identical stimuli. J Neurosci Res 85:3340–3346
46. Schaller B, Xin L, O'Brien K, Magill AW, Gruetter R (2014) Are glutamate and lactate increases ubiquitous to physiological activation? A 1H functional MR spectroscopy study during motor activation in human brain at 7Tesla. *NeuroImage* 93, 138–145
47. Boillat Y, Xin L, van der Zwaag W, Gruetter R (2020) Metabolite concentration changes associated with positive and negative BOLD responses in the human visual cortex: A functional MRS study at 7 Tesla. J Cereb Blood Flow Metab 40:488–500
48. Rae CD et al (2024) Brain energy metabolism: A roadmap for future research. J Neurochem 168:910–954
49. Mohammadi H et al (2024) Unveiling Glutamate Dynamics: Cognitive Demands in Human Short-Term Memory Learning Across Frontal and Parieto-Occipital Cortex: A Functional MRS Study. J Biomed Phys Eng 14:519–532

50. Vijayakumari AA et al (2020) Glutamatergic response to a low load working memory paradigm in the left dorsolateral prefrontal cortex in patients with mild cognitive impairment: a functional magnetic resonance spectroscopy study. Brain Imaging Behav 14:451–459
51. Caddye E et al (2026) Functional MRS uncovers age-related alterations in cerebral lactate dynamics during emotional-cognitive engagement, revealing metabolic vulnerability in the dACC. J Cereb Blood Flow Metab 0271678X261472101. 10.1177/0271678X261472101
52. Oeltzschner G et al (2019) Neurometabolites and associations with cognitive deficits in mild cognitive impairment: a magnetic resonance spectroscopy study at 7 Tesla. Neurobiol Aging 73:211–218
53. Sonnay S et al (2018) Astrocytic and neuronal oxidative metabolism are coupled to the rate of glutamate–glutamine cycle in the tree shrew visual cortex. Glia 66:477–491
54. Rothman DL, De Feyter HM, de Graaf RA, Mason GF, Behar K (2011) L. 13C MRS studies of neuroenergetics and neurotransmitter cycling in humans. NMR Biomed 24:943–957
55. Cappell KA, Gmeindl L, Reuter-Lorenz PA (2010) Age differences in prefontal recruitment during verbal working memory maintenance depend on memory load. Cortex J Devoted Study Nerv Syst Behav 46:462–473
56. Rypma B, Berger JS, Genova HM, Rebbechi D, D'Esposito M (2005) Dissociating age-related changes in cognitive strategy and neural efficiency using event-related fMRI. Cortex J Devoted Study Nerv Syst Behav 41:582–594
57. Schneider-Garces NJ et al (2010) Span, CRUNCH, and beyond: working memory capacity and the aging brain. J Cogn Neurosci 22:655–669
58. Zarahn E, Rakitin B, Abela D, Flynn J, Stern Y (2007) Age-related changes in brain activation during a delayed item recognition task. Neurobiol Aging 28:784–798
59. Metzak PD et al (2012) Decreased efficiency of task-positive and task-negative networks during working memory in schizophrenia. Schizophr Bull 38:803–813
60. Pantano P, Mainero C, Caramia F (2006) Functional brain reorganization in multiple sclerosis: evidence from fMRI studies. J Neuroimaging Off J Am Soc Neuroimaging 16:104–114
61. Ramage AE, Tate DF, New AB, Lewis JD, Robin DA (2018) Effort and Fatigue-Related Functional Connectivity in Mild Traumatic Brain Injury. Front Neurol 9:1165
62. Sinopoli KJ et al (2014) Imaging 'brain strain' in youth athletes with mild traumatic brain injury during dual-task performance. J Neurotrauma 31:1843–1859
63. Yang J et al (2020) Connectomic Underpinnings of Working Memory Deficits in Schizophrenia: Evidence From a replication fMRI study. Schizophr Bull 46:916–926
64. Iadecola C (2017) The Neurovascular Unit Coming of Age: A Journey through Neurovascular Coupling in Health and Disease. Neuron 96:17–42
65. Anand C, Khatib D, Dahle C, Raz N, Stanley JS (2019) Age Differences in Hippocampal Glutamate Modulation During Object-Location Encoding: Evidence From Proton Functional Magnetic

Resonance Spectroscopy (1H-FMRS). Biol Psychiatry 85:S298

66. Nasreddine ZS et al (2005) The Montreal Cognitive Assessment, MoCA: A Brief Screening Tool For Mild Cognitive Impairment. J Am Geriatr Soc 53:695–699
67. Kessler RC et al (2002) Short screening scales to monitor population prevalences and trends in non-specific psychological distress. Psychol Med 32:959–976
68. Corrigan JD, Hinkeldey NS (1987) Relationships between parts A and B of the Trail Making Test. J Clin Psychol 43:402–409
69. Scarpina F, Tagini S (2017) The Stroop Color and Word Test. Front Psychol 8
70. Jaeger J (2018) Digit Symbol Substitution Test: The Case for Sensitivity Over Specificity in Neuropsychological Testing. J Clin Psychopharmacol 38:513
71. Prigatano GP, Amin K (1993) Digit Memory Test: unequivocal cerebral dysfunction and suspected malingering. J Clin Exp Neuropsychol 15:537–546
72. Silva PHR, Spedo CT, Barreira AA, Leoni RF (2018) Symbol Digit Modalities Test adaptation for Magnetic Resonance Imaging environment: A systematic review and meta-analysis. Mult Scler Relat Disord 20:136–143
73. Xiao Y et al (2025) A graphical pipeline platform for MRS data processing and analysis: MRSpecLAB. Front Neuroimaging 4

Table

Table 1 is available in the Supplementary Files section.

Figures

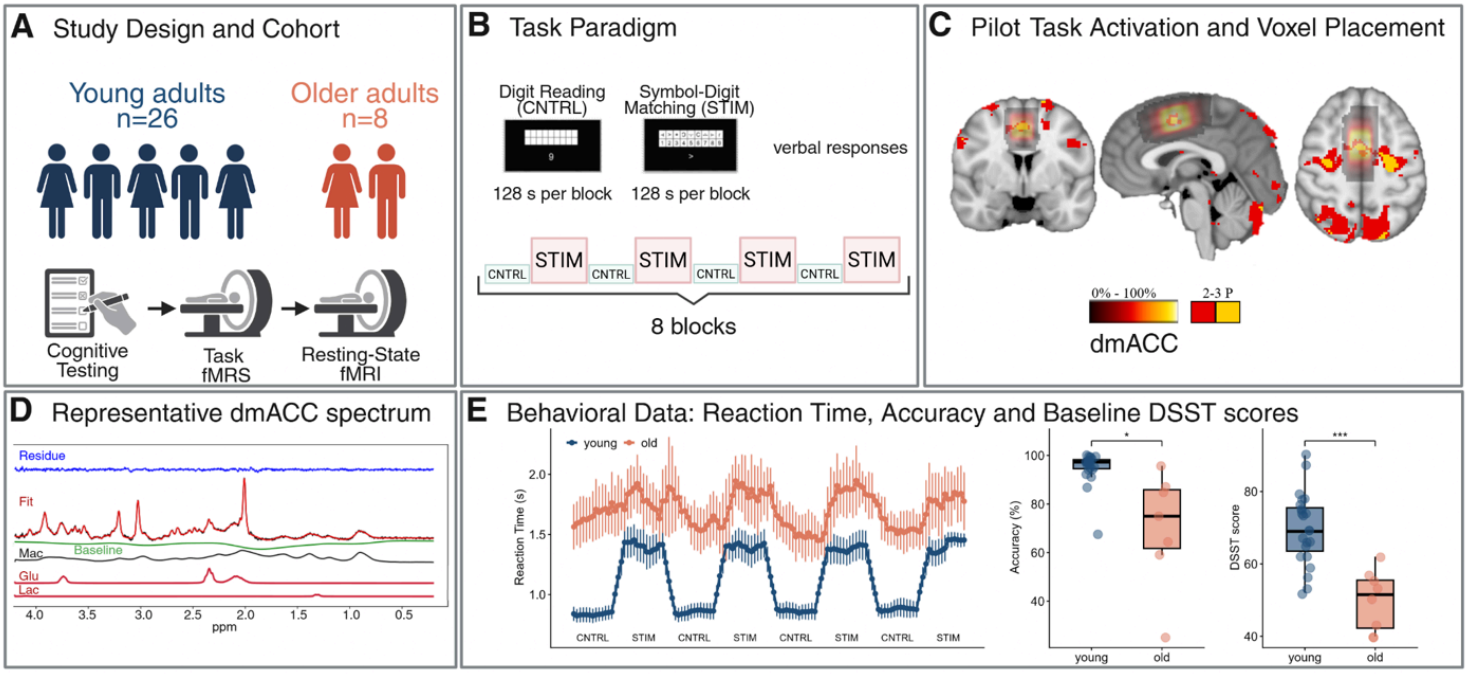


Figure 1

Study design, task paradigm and behavioural measures. A, Young (n = 26) and older (n = 8) adults completed cognitive testing, task functional MR spectroscopy (fMRS) and resting state fMRI. **B,** During scanning, participants alternated between digit reading (control; CNTRL) and symbol–digit matching (stimulation; STIM) across eight 128 s blocks, giving verbal responses. **C,** BOLD-based pilot task activation maps and placement of the dorsomedial anterior cingulate cortex (dmACC) spectroscopy voxel. **D,** Representative dmACC MR spectrum and fitted components. **E,** Reaction time across the task, accuracy by age group and baseline Digit Symbol Substitution Test (DSST) scores. Error bars in the reaction time plot show variability.

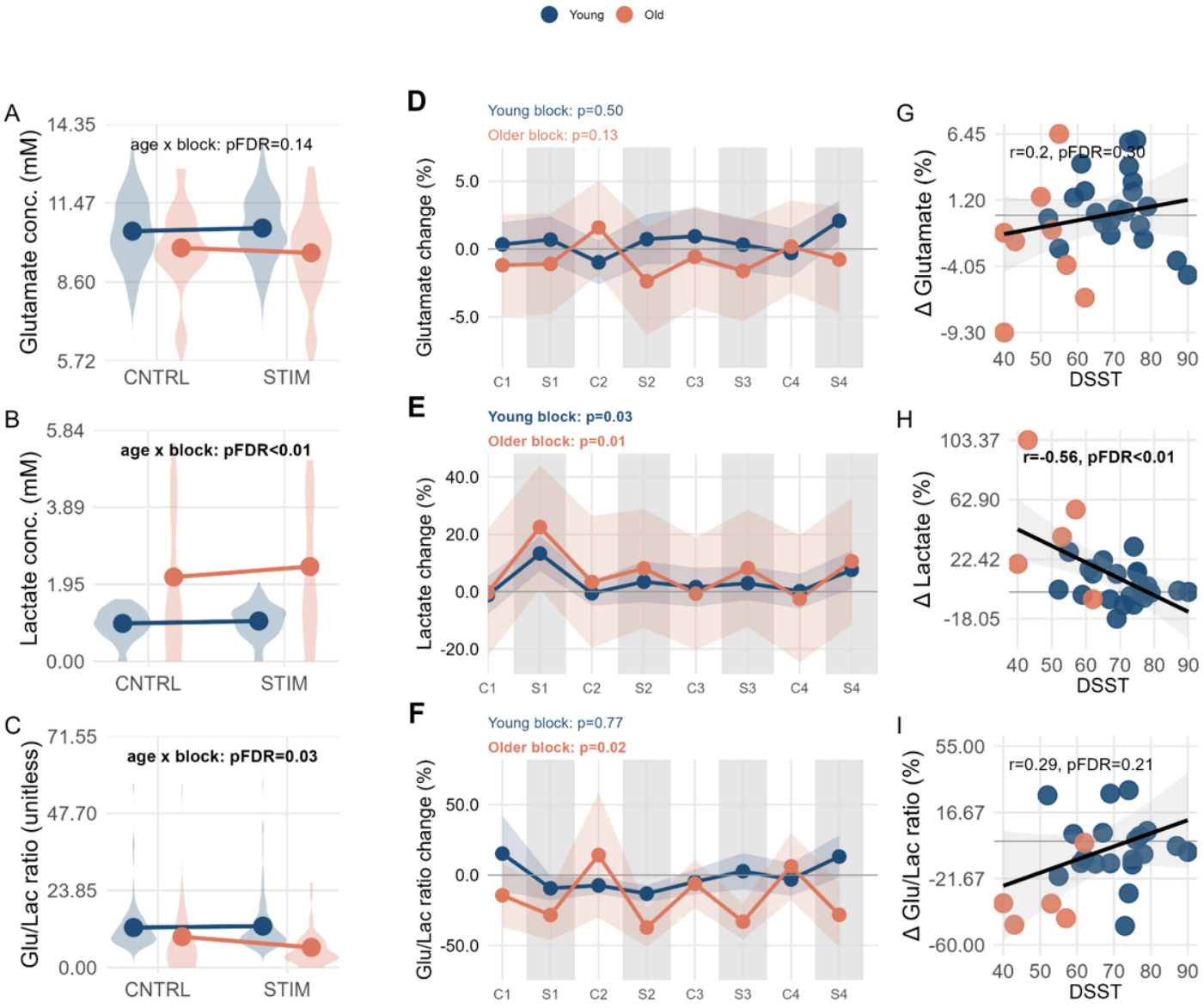


Figure 2

Task-related metabolite dynamics and associations with processing speed. A–C, Glutamate, lactate and Glu/Lac during control (**CNTRL**) and stimulation (**STIM**) in younger (**blue**) and older (**orange**)

participants. The initial control block is excluded. Violin plots show distributions; points show group means. Annotations report FDR-adjusted age-by-condition interaction p-values. **D–F,** Block-wise detrended responses expressed as percentage changes relative to the mean CNTRL concentration or ratio within each age group. Gray shading indicates stimulation; points and colored bands show group means ± SEM. Annotations labelled “Block” report within-age condition tests across all eight blocks. **G–I**, Task-related percentage changes plotted against baseline DSST scores, with regression lines and confidence bands. Larger lactate responses were associated with lower DSST scores (r = −0.56, FDR-adjusted p < 0.01); glutamate and Glu/Lac associations were nonsignificant.

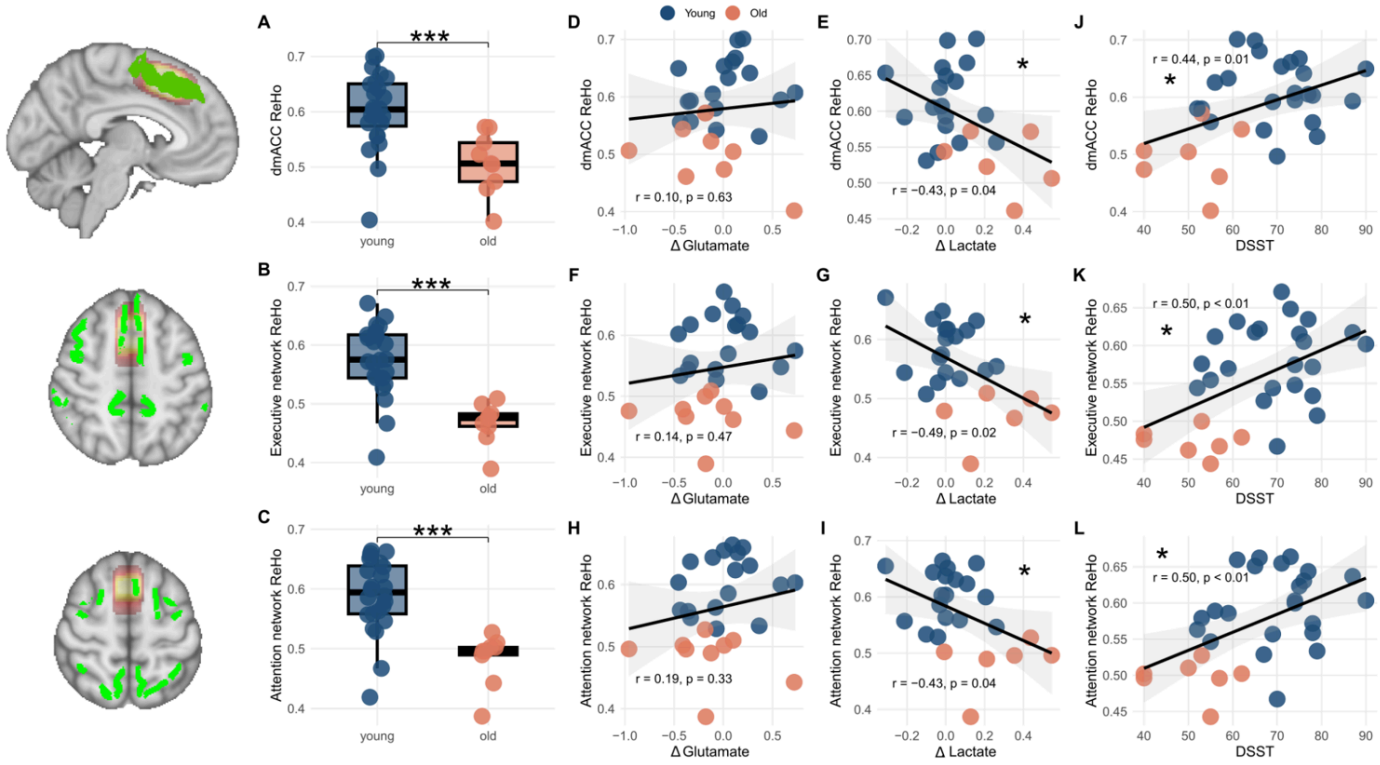


Figure 3

Resting-state regional homogeneity, task-related metabolite changes and processing speed. Anatomical images at left show the dorsomedial anterior cingulate cortex (dmACC), executive network and attention network regions of interest in green, with the MRS voxel outlined in translucent red. **A–C,** Resting-state regional homogeneity (ReHo) was lower in older (**orange**) than younger (**blue**) participants in all three regions. Points represent participants; boxes show medians and interquartile ranges. **D, F, H,** Task-related changes in glutamate were not significantly associated with ReHo. **E, G, I**, Greater lactate increases were associated with lower ReHo in the dmACC (r = −0.43, p = 0.04), executive network (r = −0.49, p = 0.02) and attention network (r = −0.43, p = 0.04). **J–L**, Higher ReHo was associated with higher Digit Symbol Substitution Test (DSST) scores in the combined sample (dmACC: r = 0.44, p = 0.01; executive and attention networks: r = 0.50, p < 0.01 for each). *Lines show linear fits with shaded 95% confidence intervals. Reported correlations are exploratory; p-values shown in the plots are unadjusted.*

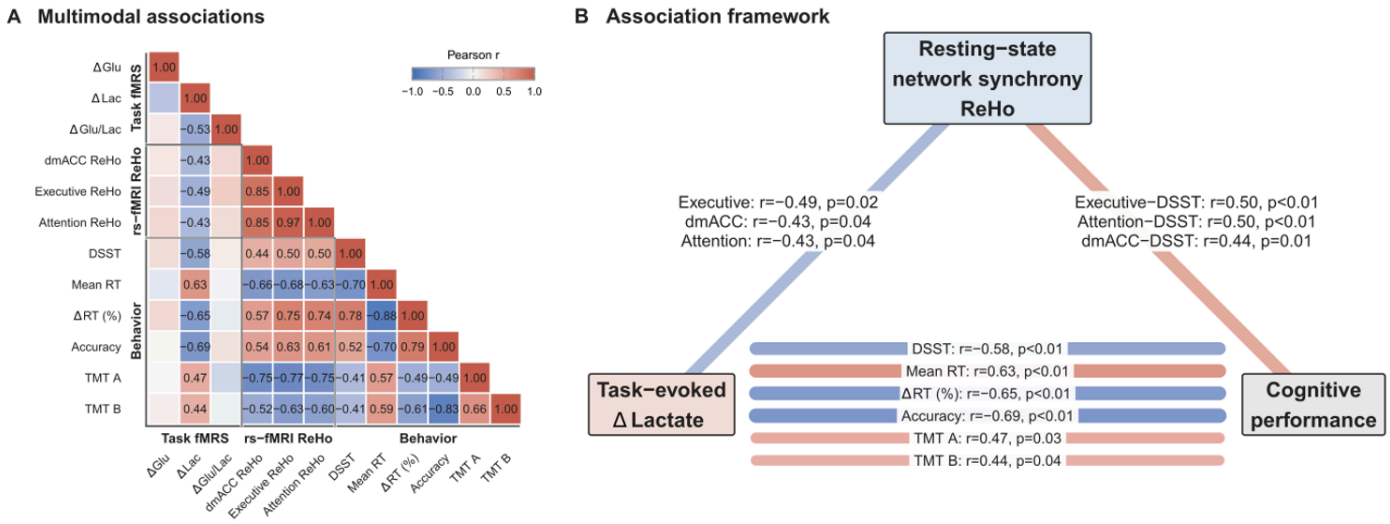


Figure 4

Multimodal associations between task-evoked neurochemistry, resting-state network organization, and cognitive performance. A, Lower-triangular Pearson correlation matrix showing task-related changes in glutamate (ΔGlu), lactate (ΔLac) and the Glu/Lac ratio; regional homogeneity (ReHo) in the dmACC, executive, and attention networks; and behavioral measures (DSST, reaction time, reaction time change, accuracy, TMT-A, and TMT-B). Tile color indicates the direction and magnitude of Pearson r (red, positive; blue, negative). Numerical r values are displayed when the unadjusted p value is <0.10; unlabelled tiles also represent calculated correlations. **B,** Exploratory summary of associations among ReHo, task-evoked lactate change, and cognitive performance. Labels report r and unadjusted p values; line color indicates correlation direction and line width reflects magnitude. Larger lactate responses were associated with lower ReHo and poorer performance, whereas higher ReHo was associated with better DSST performance. Higher DSST and accuracy scores indicate better performance; longer reaction and Trail Making times indicate poorer performance. Associations across the combined sample may partly reflect differences between age groups.

Supplementary Files

This is a list of supplementary files associated with this preprint. Click to download.

- MANUSCRIPTPROCSPEEDsupp.docx
- Table1.docx